Journal for ImmunoTherapy of Cancer

Characterization of the treatment-naive immune microenvironment in melanoma with *BRAF* mutation

Minyu Wang ,[1,2] Soroor Zadeh,[3,4] Angela Pizzolla,[1,2] Kevin Thia,[1,5] David E Gyorki,[6] Grant A McArthur,[2,7] Richard A Scolyer ,[8,9] Georgina Long,[10,11] James S Wilmott,[10,12] Miles C Andrews ,[13] George Au-Yeung,[2,7] Ali Weppler,[7] Shahneen Sandhu,[2,7] Joseph A Trapani,[1,2] Melissa J Davis,[3,4] Paul Joseph Neeson [1,2]

To cite: Wang M, Zadeh S, Pizzolla A, *et al*. Characterization of the treatment-naive immune microenvironment in melanoma with *BRAF* mutation. *Journal for ImmunoTherapy of Cancer* 2022;**10**:e004095. doi:10.1136/jitc-2021-004095

► Additional supplemental material is published online only. To view, please visit the journal online (http://dx.doi.org/10.1136/jitc-2021-004095).

MW and SZ contributed equally.

MJD and PJN are joint senior authors.

Accepted 14 March 2022

For numbered affiliations see end of article.

Correspondence to
Dr Paul Joseph Neeson; paul.neeson@petermac.org

Dr Melissa J Davis; davis.m@wehi.edu.au

ABSTRACT

Background Patients with *BRAF*-mutant and wild-type melanoma have different response rates to immune checkpoint blockade therapy. However, the reasons for this remain unknown. To address this issue, we investigated the precise immune composition resulting from *BRAF* mutation in treatment-naive melanoma to determine whether this may be a driver for different response to immunotherapy.

Methods In this study, we characterized the treatment-naive immune context in patients with *BRAF*-mutant and *BRAF* wild-type (*BRAF*-wt) melanoma using data from single-cell RNA sequencing, bulk RNA sequencing, flow cytometry and immunohistochemistry (IHC).

Results In single-cell data, *BRAF*-mutant melanoma displayed a significantly reduced infiltration of $CD8^+$ T cells and macrophages but also increased B cells, natural killer (NK) cells and NKT cells. We then validated this finding using bulk RNA-seq data from the skin cutaneous melanoma cohort in The Cancer Genome Atlas and deconvoluted the data using seven different algorithms. Interestingly, *BRAF*-mutant tumors had more $CD4^+$ T cells than *BRAF*-wt samples in both primary and metastatic cohorts. In the metastatic cohort, *BRAF*-mutant melanoma demonstrated more B cells but less $CD8^+$ T cell infiltration when compared with *BRAF*-wt samples. In addition, we further investigated the immune cell infiltrate using flow cytometry and multiplex IHC techniques. We confirmed that *BRAF*-mutant melanoma metastases were enriched for $CD4^+$ T cells and B cells and had a co-existing decrease in $CD8^+$ T cells. Furthermore, we then identified B cells were associated with a trend for improved survival (p=0.078) in the *BRAF*-mutant samples and Th2 cells were associated with prolonged survival in the *BRAF*-wt samples.

Conclusions In conclusion, treatment-naive *BRAF*-mutant melanoma has a distinct immune context compared with *BRAF*-wt melanoma, with significantly decreased $CD8^+$ T cells and increased B cells and $CD4^+$ T cells in the tumor microenvironment. These findings indicate that further mechanistic studies are warranted to reveal how this difference in immune context leads to improved outcome to combination immune checkpoint blockade in *BRAF*-mutant melanoma.

Key messages

- Patients with *BRAF*-mutant versus *BRAF* wild-type metastatic melanoma have different response rates to immune checkpoint blockade treatment. The reasons for this are currently unclear. In treatment-naive patients, we revealed that *BRAF*-mutant melanoma immune context is distinct from that of wild-type melanoma in both primary and metastatic disease, and this has prognostic significance. These findings indicate further mechanistic studies are warranted to reveal why the *BRAF*-mutant melanoma responds better to dual immune checkpoint blockade, ultimately leading to new predictive biomarkers and improved stratification of patients for therapy.

INTRODUCTION

Melanoma is one of the leading causes of cancer-related mortality worldwide. Up to 20% of patients develop advanced/metastatic disease, and historically the 10-year survival rate in patients with advanced melanoma is approximately 10%.[1] Alterations in several oncogenic driver genes, including genes encoding *NRAS* and the serine/threonine kinase *BRAF*, have been identified in melanoma.[2] Up to 40% of melanomas carry an activating *BRAF* mutation, and 90% of reported *BRAF* mutations result in a substitution of glutamic acid for valine at amino acid 600.[3] Among these, around 70% are V600E, 20% are V600K and the remainder are rarer mutations, including V600R, V600D, V600E2, V600G, V600M, V600A and V600L.[4] *BRAF* V600 mutations constitutively activate *BRAF* and downstream signal transduction in the mitogen-activated protein kinase (MAPK) pathway.[5] Targeting the MAPK pathway with combined BRAF and MEK inhibition induces rapid responses and improves survival[6 7] in patients with activating *BRAF*V600 mutations,

however, disease control is often not sustained, with a median progression-free survival of approximately 12 months.[8–10]

Recently, immune checkpoint inhibitors (ICIs), including monoclonal antibodies (mAbs) against programmed cell death-1 (PD-1) and programmed cell death-ligand 1, have demonstrated impressive antitumor effects in melanoma. The 5-year overall survival rates are around 34%–41% and 44% in patients treated with pembrolizumab[11] and nivolumab,[12] respectively. The 5-year overall survival improves to 52% when treated with nivolumab plus ipilimumab, an mAb targeting cytotoxic T-lymphocyte-associated antigen 4 (CTLA4),[12] but with a corresponding increase in toxicity.[12] Notably, the 5-year overall survival with nivolumab-plus-ipilimumab was higher in patients with a *BRAF* mutation at 60%, in contrast to 48% in patients without *BRAF* mutations.[12] This suggests that the treatment-naive immune context in melanoma with *BRAF* mutations is distinct from those without *BRAF* mutations. More interestingly, a recent study demonstrated that an interferon γ gene expression signature was a prognostic factor and was of relevance for stratifying patients with respect to clinical benefit from BRAF and MEK inhibitors.[13] These data further emphasize the critical role of the immune response in determining the clinical benefit from not only ICIs but also targeted therapy. Thus, an in-depth characterization of the treatment-naive immune context in melanoma with *BRAF* mutations is needed. Previous in vitro studies demonstrated that the MAPK signaling pathway can induce immune evasion in human melanoma cells,[14] and oncogenic *BRAF* promoted stromal cell-mediated immune suppression in melanoma.[15] Studies also show that BRAF and/or MEK inhibitors have beneficial effects in boosting the antitumor immune response through increased immune-stimulatory cytokine levels and increased intratumoral effector T cell infiltration and activity.[16–18] However, the treatment-naive immune context in *BRAF*-mutant melanoma has not been investigated systematically. A better understanding of the immune phenotypes associated with *BRAF* mutations would benefit the rational development of optimal therapy for patients with melanoma.

MATERIALS AND METHODS

Single-cell transcriptomic analysis

Normalized gene expression levels in log reads per kilobase of transcript, per million mapped reads and clinical metadata for single-cell RNA sequencing (scRNA-seq) measurements from patients with metastatic melanoma[19] were downloaded from a published study via Gene Expression Omnibus, through accession number GSE72056. The study included measurements from a total number of 4645 cells from 19 patients: 8 patients wt for *NRAS* and *BRAF*, 5 patients with *NRAS* mutation, 4 with *BRAF* V600 mutations (*BRAF*-V600E=3, *BRAF*-V600K=1) and 2 patients with unknown mutation status. Cells annotated as malignant by the study were removed. Although the cell type identities were already determined for the 3388 non-malignant cells by this study, we took advantage of recent developments in the field and applied a reference-based strategy to re-annotate the cell types. We mapped the non-malignant metastatic melanoma single cells to a comprehensive reference of immune cell types using scArches.[20] The reference dataset was generated from lung, PBMCs and bone marrow immune and epithelial cells, integrating cell types across 17 different studies as described by Wolf *et al*.[21] We ran scArches in the default mode, but changed the loss function to the sum of squared of the errors as we were using normalized log expression values. We merged the reference dataset and the metastatic melanoma dataset using 2000 highly variable genes using scanpy.[21] Briefly, scArches estimates latent spaces where the reference and query melanoma data set can be optimally aligned. Then, a weighted k-nearest neighbor (KNN) classifier is used to predict the identity of cells in a neighborhood on that latent integrated space. We used a weighted KNN classifier that predicts cell type annotation in the latent integrated space using five nearest neighbors with less than 5% prediction uncertainty.

The reference-based approach to cell type annotation resulted in the identification of more diverse cell types compared with the marker-based annotation applied by the original study.[19] We then tested for differences in the abundance of cell types between cells from *BRAF* mutation and *BRAF* wild-type (*BRAF*-wt) samples. For each predicted cell type, we tested if there is a difference in the number of counts of *BRAF*-mutant cells and *BRAF*-wt cells using Fisher's exact test in R.

Differential gene expression and pathway analysis using the bulk RNA-seq from The Cancer Genome Altas (TCGA) skin cutaneous melanoma (SKCM) cohort

Raw bulk RNA-seq data for TCGA SKCM primary and metastatic tumors and clinical annotation were downloaded using the TCGAbiolinks Bioconductor package.[22] RNA-seq counts were filtered by expression, the log counts per million (logCPM) transformed and trimmed mean of M-values normalized[23] using edgeR.[24] Differential gene expression analyses were performed in each primary and metastatic cohorts using the quasi-likelihood pipeline of edgeR.[25] Briefly, gene-wise negative binomial dispersion values were estimated. A quasi-likelihood negative binomial log-linear model was fitted for each gene. The p value for differential expression was determined by the quasi-likelihood F-test and adjusted for multiple hypotheses testing. Genes with a false discovery rate <0.05 were determined as differentially expressed between *BRAF*-mutant and *BRAF*-wt samples. We tested for the enrichment of MsigDB Hallmark gene set collection in *BRAF*-mutant cases compared with *BRAF*-wt cases using fry[25] in limma R/Bioconductor package.[26] The mutation subtypes for TCGA SKCM samples were retrieved from online supplemental table of the original study by Thorsson *et al*.[27]

Cell type analysis using the bulk RNA-seq from the TCGA SKCM cohort

To quantify differences in immune decomposition between *BRAF*-mutant and *BRAF*-wt tumors, we first quantified infiltrating immune cell types in each sample using multiple bulk RNA-seq immune deconvolution methods to leverage the strengths of various deconvolution algorithms. The abundances of immune cell types in each sample were estimated using quanTIseq,[28] TIMER,[29] CIBERSORT,[30] MCPCounter,[31] XCell,[32] EPIC[33] and ImmuCellAI[34] deconvolution algorithms implemented in immunedeconv R package.[35]

To compare the infiltrating immune cell types between *BRAF*-mutant and *BRAF*-wt samples, we first fitted a logistic regression model to cell type scores estimated by each deconvolution algorithm using R package glmnet.[36–39]

This provided us with regression coefficients from multiple models (one model for each deconvolution approach) that reflect the association between *BRAF* mutation status and the cell type scores estimated by each deconvolution method.

We then borrowed strengths between different deconvolution algorithms by stacking the individual logistic regression coefficients (also called weights). We fitted a feature-weighted elastic net (fwelnet) model to stack the logistic regression models fitted to scores from individual deconvolution methods.[40] This is equivalent to fitting a meta-model to individual models to borrow strengths between various deconvolution approaches. We obtained weights for each cell type in each deconvolution approach using this approach, some of which were zero. This resulted in the selection of only a subset of cell types across various deconvolution algorithms that are most likely to contribute to differences between *BRAF*-mutant and *BRAF*-wt samples, both in a positive and in a negative way. We simply took the weighted average of regression coefficients from models fitted to each deconvolution method as the final (stacked) regression coefficients, where weights are the coefficients estimated by the fwelnet model, only for cell types selected by this meta-model. We, therefore, were able to identify cell types that are most relevant to the difference between *BRAF*-mutant and *BRAF*-wt sample, and we quantified this difference by a single value obtained by stacking regression coefficients from individual models fitted to each deconvolution approach, weighted by the relevance of each deconvolution approach. The regularization parameter, the shrinkage operator, in fwelnet model was determined by 10-fold cross-validation. This model fitting process was applied to primary and metastatic cohorts separately.

Patient samples for flow cytometry and multiplex immunohistochemistry (IHC)

Patients undergoing surgical resection of melanoma metastases (as clinically indicated) were enrolled in a prospective protocol after approval from the Peter MacCallum Cancer Center (PMCC) Human Research Ethics Committee (HREC) under approval no 13/141. All methods performed in this study were carried out in accordance with relevant guidelines and regulations under this approval. Clinical data were collected prospectively from the patient, and missing data were extracted from the medical record. Online supplemental table 1 provides details of each patient's treatment-naive melanoma metastasis.

Flow cytometry

Following tumor excision, a representative fragment of tumor measuring approximately 1 cm^3 was transferred fresh and sterile to the laboratory for study. Briefly, the tumor was initially divided into segments and then finely diced into RPMI1640 (Gibco) containing 1 mg/mL collagenase type 4 (Worthington Biochemical, Lakewood, New Jersey, USA), 30 U/mL DNase (Sigma-Aldrich Pty, Sydney, NSW, Australia) and incubated for 30 minutes at 37°C on a rocker. Digested tumor pieces were teased through a 100 µm sieve, the sieve irrigated with RPMI1640 supplemented with 10% heat-inactivated fetal calf serum (RP-10) and the cells collected into a 50 mL conical tube. Pelleted cells were resuspended in RP-10 and used for flow cytometry analysis.

Approximately 2×10^5 cells were plated in V-bottom 96-well plates and spun down. First cells were stained with viability dye LIVE/DEAD Fixable Near-IR Dead Cell (ThermoFisher) diluted in phosphate-buffered saline (PBS) for 10 min at room temperature in the dark. After one wash in FACS buffer (PBS (Ca++/Mg ++free), 2% fetal bovine serum, 2 mM EDTA), the FC receptors were blocked with Human TruStain (BD Biosciences, San Diego, California, USA) for 10 min at room temperature. Cells were stained with fluorochrome-conjugated mAbs for extracellular markers for 30 min at 4°C in FACS buffer. After one wash in FACS buffer, cells were fixed with eBioscience Foxp3/Transcription Factor Staining Buffer Set (Invitrogen) and stained with intracellular antibodies for 30 min at 4°C in permeabilization wash buffer. After two washes in permeabilization wash buffer and one in FACS buffer, the cells were acquired on BD Symphony (BD Biosciences) and data analyzed using FlowJo V.10 software (Treestar, Seattle, California, USA).

Antibodies used in this study included CD45-BV510, CD8-BV605, PD-1-BV785, CCR7-BV711, CD4-AlexaFluor700, CD39-APC, LAG3-PE Dazzle594, CTLA4-PercpCy5.5, CD11c-APC, HLA-ABC PercPCy5.5 (BioLegend, San Diego, California, USA); HLA-ABC-PE, CD3 BUV395, CD45RA-FITC, CD8-BV805, CD69 PE-cy7, CD103-BV421, CD19-BV450, CD14-PE-CF594, CD56-FITC (BD Biosciences) and Foxp3-PE (eBioscience, San Diego, California, USA). A representative example of the gating strategy of antigen-presenting cells and T cells is shown in online supplemental figure 1.

Multiplex IHC

Three micrometer sections of FFPE tissue on super frost plus slides were deparaffinized and rehydrated by serial passage through changes of xylene and graded ethanol

for multiplex IHC staining. Full details for staining, imaging, cell segmentation, data processing and quality control were described in a previous study.[41]

Selection of cell type signatures predicting survival outcomes in TCGA SKCM cohort

To identify immune cell types associated with survival differences within TCGA patients with *BRAF* mutation (ie, cell type that is differentially infiltrated between *BRAF* patients with excellent and poor survival outcomes), we applied a penalized Cox proportional hazard model[37] to the scores of cell type signatures selected by the fwelnet model. The optimal value for the shrinkage penalty was selected in 10-fold cross-validation. This resulted in a subset of cell type signatures selected by the fwelnet model that are relevant to survival outcomes in *BRAF* cases. The same procedure was applied to *BRAF*-wt cases.

Statistical analyses

Data analyses and representations were performed either with the R software or Prism (GraphPad V.8.0, San Diego, California, USA). Statistical analyses for two groups were performed using the Mann-Whitney U test for the cohort with a small sample size of less than 20 and Student's t-test for the cohort with a large sample size. Results are shown as the mean+SEM. Fisher's exact test was used for categorical data. A p value ≤0.05 was considered statically significant. Kaplan-Meier curves and Cox proportional HRs were performed using survival[42] and survminer[43] R packages.

RESULTS

Study design

In this study, we systematically examined the tumor microenvironment immune composition in melanoma samples with or without *BRAF* V600 mutations (figure 1). We examined data from three independent cohorts using scRNA-seq, bulk RNA sequencing (bulk RNA-seq), flow cytometry and multiplex IHC. We next used TCGA SKCM data and correlated the immune compositions with the patients' outcome to identify immune biomarkers of prognosis in patients with melanoma with or without *BRAF* mutation.

Immune composition differs between *BRAF*-mutant and wild-type melanomas

We re-analyzed the single-cell RNA-seq profiles from a total of 4645 malignant, immune and stromal cells isolated from 19 freshly procured human melanoma tumors[19]: 8 patients wt for *NRAS* and *BRAF*, 5 patients with *NRAS* mutation, 4 with *BRAF* V600 mutations (*BRAF*-V600E=3, *BRAF*-V600K=1) and 2 patients with unknown mutation status. This cohort included 10 metastases to lymphoid tissues (nine to lymph nodes and one to the spleen), eight to distant sites (five to subcutaneous/intramuscular tissue and three to the gastrointestinal tract) and one primary acral melanoma. We utilized the recently developed comprehensive reference of immune cell types scArches[20] (figure 2A) and annotated the 3388 non-malignant cells in the study. The reference-based approach to cell type annotation identified more diverse cell types compared with the marker-based annotation applied by the original study. The single-cell data was projected in two-dimensional space through uniform manifold approximation and projection with different *BRAF* status in figure 2B and labeled with different cell types (figure 2C and online supplemental figure 2). We then tested for differences in the abundance of the immune cell types between cells from melanoma samples with or without *BRAF* mutation (figure 2D). *BRAF*-mutant melanoma displayed significantly reduced $CD8^+$ T cells and macrophages, but an increased number of B cells, natural killer (NK) cells and NKT cells (figure 2D).

We then studied the differences in the gene expression and molecular signaling pathways between the *BRAF*-mutant and *BRAF*-wt tumors using the 471 melanoma tumors from TCGA SKCM. We separated the primary tumors from the metastatic tumors for the analysis, as we hypothesized the gene profile and cell type composition were different between these two types. This analysis showed more genes were differentially expressed between the *BRAF*-mutant and *BRAF*-wt tumors in the metastatic samples than in the primary samples (figure 3A). We then used the 50 hallmark gene sets of the Molecular Signatures Database (MSigDB)[44] for molecular signaling pathway analysis. In line with the previous results, the 50 gene set expression variations for both *BRAF*-mutant and *BRAF*-wt tumors did not demonstrate a significant difference in the primary cohort. However, striking differences in signaling pathways were identified in the metastatic tumor cohort. Within these, transforming growth factor-ß signaling, inflammatory response, IL6-JAK-STAT3 signaling and IL2-STAT5 signaling were enriched in *BRAF*-mutant tumors (figure 3B). Taken together, the differences in gene expression and signaling pathways between *BRAF*-mutant and *BRAF*-wt samples were more evident when melanoma progressed to regional metastatic disease in the TCGA SKCM cohort.

We further quantified the immune composition in each sample using various bulk RNA-seq deconvolution algorithms, including quanTIseq,[28] TIMER,[29] CIBERSORT,[30] MCPCounter,[31] XCell,[32] EPIC[33] and ImmuCellAI.[34] To comprehensively compare the infiltrating immune cell types between *BRAF*-mutant and *BRAF*-wt samples, we first fitted a logistic regression model to cell type scores estimated by each individual deconvolution algorithm. This provided us with regression coefficients from multiple models. We then leveraged the independence of multiple deconvolution algorithms to perform feature selection by stacking the individual logistic regression coefficients, also called weights, and fitted them using a fwelnet model.[40] Using this approach, we were able to obtain weights for each cell type in each deconvolution algorithm. This resulted in the selection of only a subset of cell types that are most likely to contribute to the difference, in

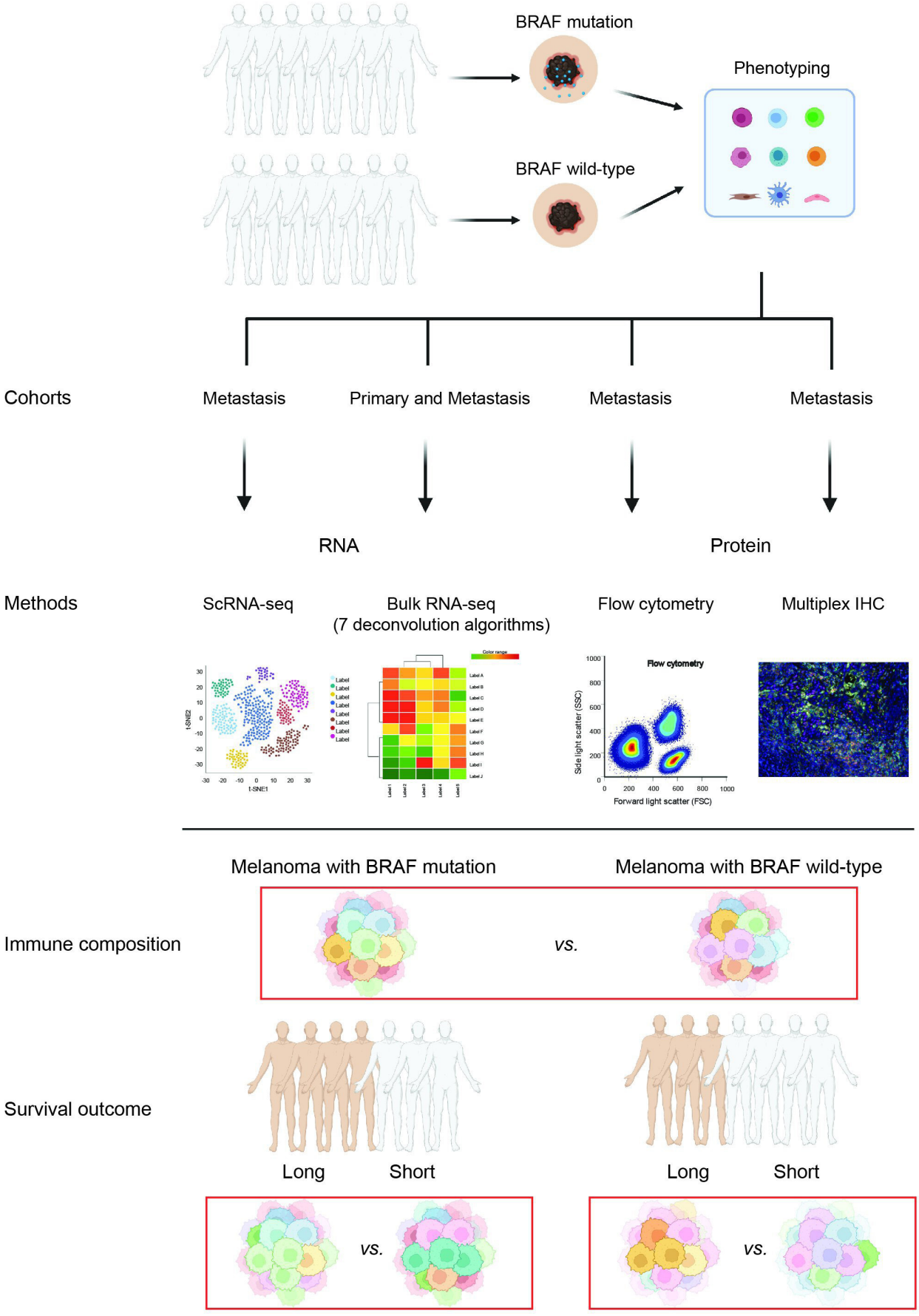

Figure 1 Schematic illustration of the experimental design in this study. CAFs, cancer-associated fibroblasts; IHC, immunohistochemistry; ScRNA seq, single-cell RNA sequencing

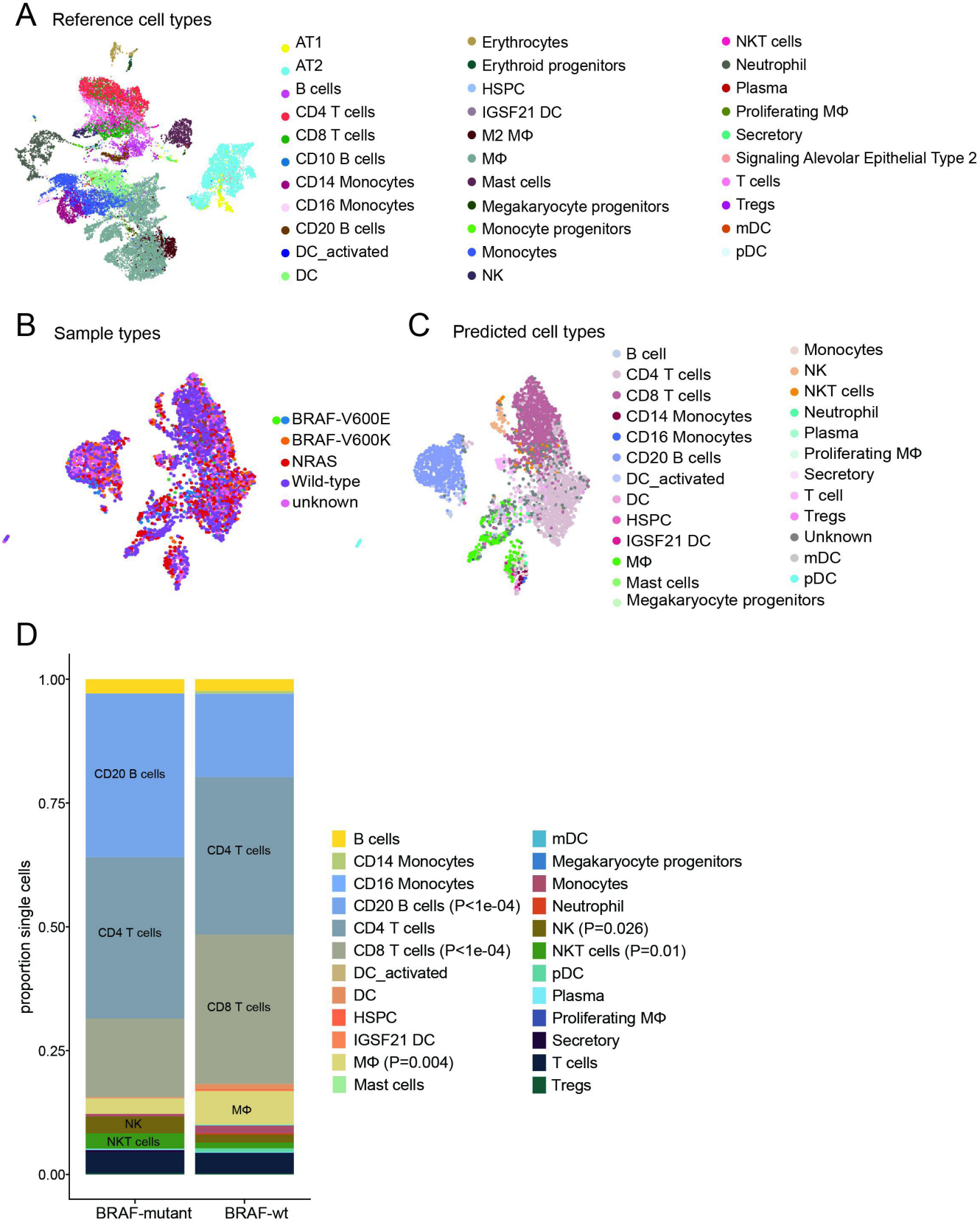

Figure 2 Single-cell transcriptomic analysis reveals the transcriptome of cells in the tumor microenvironment of melanoma samples. (A) UMAP visualization of reference cell types. (B,C) UMAP visualization of sample mutation (B) and predicted cell types (C) using scRNA-seq data of 3388 cells isolated from metastatic melanoma sample. (D) Pair-wise comparison of predicted cell types between *BRAF*-mutant and *BRAF*-wt melanoma samples. Significantly different immune cell populations are indicated by p<0.05 using Fisher's exact test. HPSC, hematopoietic stem cell; mDC, myeloid dendritic cells; MΦ, macrophages; NKT cells, natural killer T cells; pDC, plasmacytoid dendritic cells; UMAP, uniform manifold approximation and projection.

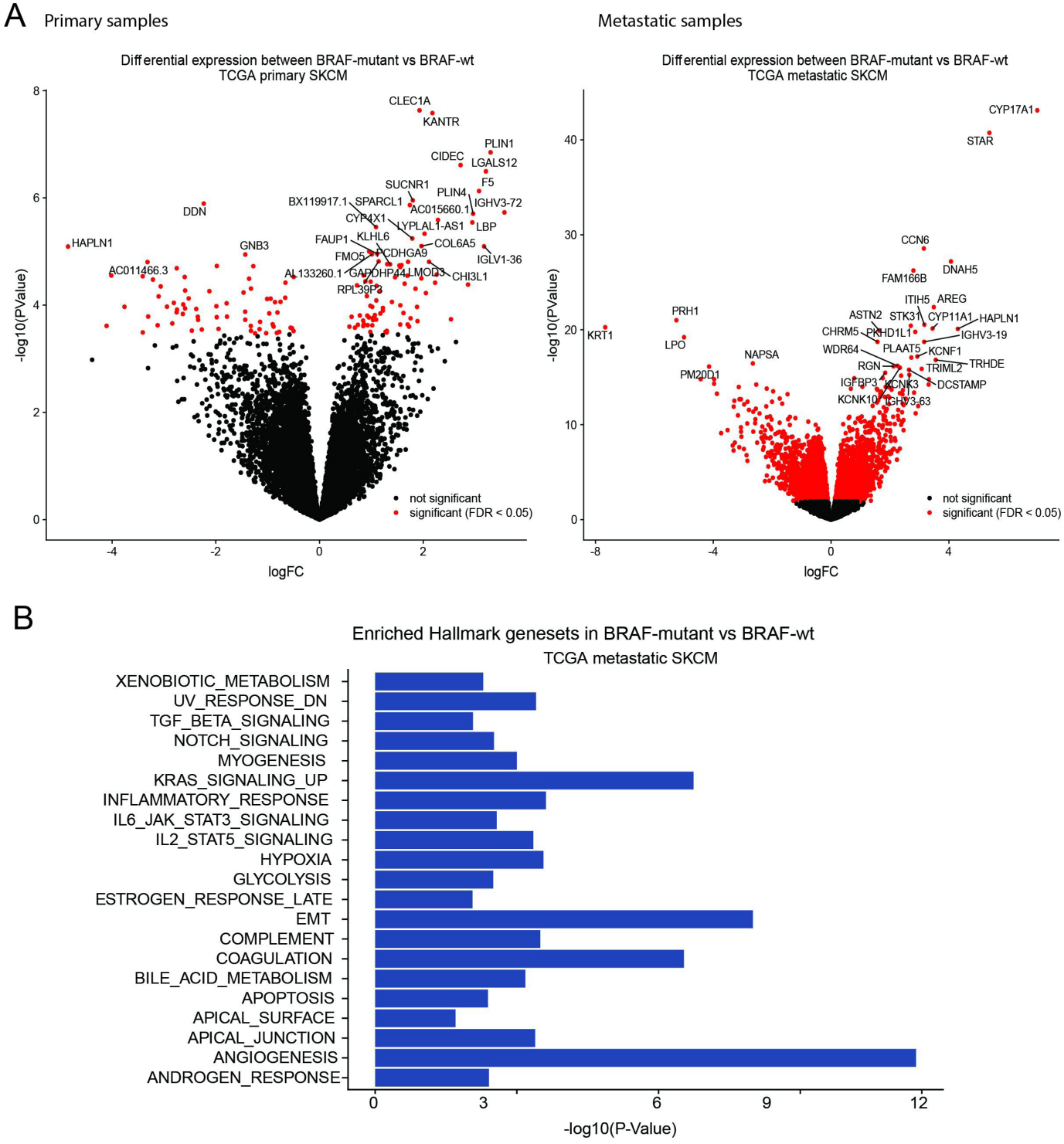

Figure 3 Differentially expressed gene and pathway analysis using the bulk RNA-seq from TCGA SKCM cohort. (A) Differential gene expression analyses were performed in primary and metastatic cohorts using the quasi-likelihood pipeline of edgeR. The p value for differential expression was determined by the quasi-likelihood F-test and adjusted for multiple hypotheses testing. Genes with FDR < 0.05 were determined as differentially expressed between *BRAF*-mutant and *BRAF*-wt samples. (B) The enrichment of MsigDB Hallmark gene set collection in *BRAF*-mutant samples compared with *BRAF*-wt samples was tested using fry in limma R/Bioconductor package. FDR, false discovery rate; SKCM, skin cutaneous melanoma; TCGA, The Cancer Genome Atlas.

either a positive or negative way, between *BRAF*-mutant and *BRAF*-wt samples. This model fitting approach was applied to primary and metastatic cohorts in the TCGA separately (figure 4A,B). Not surprisingly, some cell types predicted by different algorithms demonstrated opposite associations with *BRAF* mutation status, such as the Tregs from XCell, CIBERSORT and immuCellAI. To identify cell types that most reliably differentiate *BRAF*-mutant

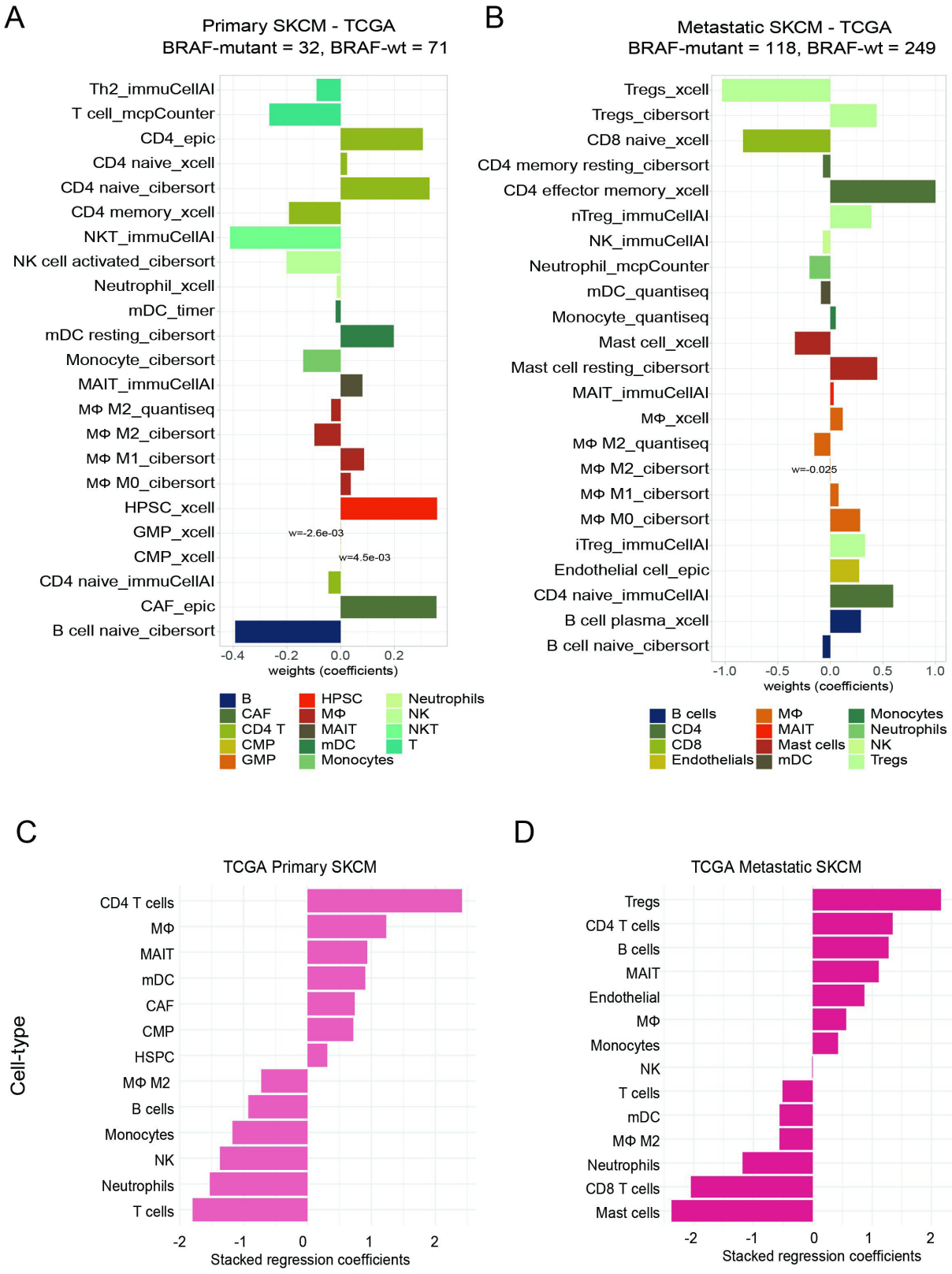

Figure 4 Cell type analysis using the bulk RNA-seq from the TCGA SKCM cohort. (A,B) The immune compositions in each sample were quantified using various bulk RNA-seq deconvolution algorithms, including quanTIseq,[28] TIMER,[29] CIBERSORT,[30] MCPCounter,[31] XCell,[32] EPIC[33] and ImmuCellAI.[34] The cell type scores calculated by a logistic regression model were stacked and fitted using a feature-weighted elastic net (fwelnet) model for the primary (A) and metastatic (B) cohorts separately. (C,D) The weighted average of regression coefficients was used as the final stacked regression coefficients for the primary (C) and metastatic (D) cohorts separately. CAF, cancer-associated fibroblast; CMP, common myeloid progenitor; GMP, granulocyte-monocyte progenitor; HPSC, hematopoietic stem cell; mDC, myeloid dendritic cells; MΦ, macrophages; NKT cells, natural killer T cells; SKCM, skin cutaneous melanoma;TCGA, The Cancer Genome Atlas.

and *BRAF*-wt samples, we took the weighted average of regression coefficients as the final stacked regression coefficients, where weights were the coefficients estimated by the fwelnet model. As a result, we observed an enrichment of $CD4^+$ T cells, macrophages, mucosal-associated invariant T (MAIT) cells, myeloid dendritic cells (mDCs), cancer-associated fibroblasts (CAFs), common myeloid progenitor (CMP) and hematopoietic stem cells in the *BRAF*-mutant samples (figure 4C). We also observed a decrease of M2 macrophages, B cells, monocytes, NK cells, neutrophils and T cells in the *BRAF*-mutant samples in the primary SKCM cohort (figure 4C). An enrichment of Tregs, $CD4^+$ T cells, B cells, MAIT, endothelial cells, macrophages, monocytes and NK cells, as well as a decrease of T cells, mDCs, M2 macrophages, neutrophils and $CD8^+$ T cells and mast cells, was observed in the *BRAF*-mutant samples in the metastatic SKCM cohort (figure 4D). Taken together, these results from a large cohort of bulk RNA-seq data were in line with the single-cell data and showed enrichment of B cells in the *BRAF*-mutant metastatic samples and enrichment of $CD8^+$ T cells in the *BRAF*-wt metastatic samples. Interestingly, $CD4^+$ T cells were enriched in *BRAF*-mutant samples in both primary and metastatic cohorts. The inconsistency of some cell types, such as macrophages and DCs, between scRNA-seq and bulk RNA-seq may be due to the loss of these cells during the fresh samples digestion required during single-cell RNA-seq sample preparation.

To validate the scRNA-seq and bulk RNA-seq data above, we re-analyzed multiplex IHC and flow cytometry data[41] to evaluate the immune cell types in a metastatic melanoma cohort, comprising seven *BRAF*-mutant and nine *BRAF*-wt samples (online supplemental table 1). Surgical resection samples from patients diagnosed with stage III or IV metastatic melanoma were collected, digested and single-cell suspensions generated for flow cytometric analysis. Notably, *BRAF*-mutant samples demonstrated significantly more B cells and $CD4^+$ T cells and less $CD8^+$ T cell infiltrates when compared with the *BRAF*-wt samples (figure 5A). This result was in line with scRNA-seq and bulk RNA-seq results. We then further characterized T cell function. Interestingly, although there were less $CD4^+$ T cells, a significant enrichment of $CD4^+$ central memory T cells was observed in the *BRAF*-wt samples when compared with the *BRAF*-mutant samples (figure 5B). There was also a trend towards more $CD8^+$ effector memory T cells in the *BRAF*-wt samples. Next, we used multiplex IHC to characterize the spatial distribution of these lymphocytes in five *BRAF*-mutant and five *BRAF*-wt samples (online supplemental table 1). We observed an increased number of $CD4^+$ T cells in the *BRAF*-mutant samples, which were predominately presented in the peri-tumoral (stroma) area instead of the intratumoral area and less $CD8^+$ T cells presented in the stroma area (online supplemental figure 3), although not significant when compared with the *BRAF*-wt samples (figure 5C). Taken together, these findings suggest that the $CD4^+$ T cells in the *BRAF*-mutant samples, although increased in number, were decreased in the central memory type and excluded from the tumor center. The $CD8^+$ T cells were decreased in number and effector memory phenotype in the *BRAF*-mutant cases.

B cells are associated with improved overall survival of patients with *BRAF*-mutant melanoma

We then investigated whether immune cell types could predict patient survival. To do this, we utilized the survival data from the TCGA SKCM cohort and applied a penalized Cox proportional hazard model to the scores of cell type signature selected by the fwelnet model. In the primary samples, the B_Cell_naive_cibersort (the naive B cell signature enumerated by CIBERSORT algorithm) was associated with improved survival in the *BRAF*-mutant tumors (figure 6A, left panel), but this association was not significant in the *BRAF*-wt samples. Instead, CAF_epic was associated with inferior survival and Th2 with improved survival in the *BRAF*-wt samples (figure 6A, right panel). In metastatic tumors, iTreg was significantly associated with an improved prognosis in the metastatic samples (figure 6B, left panel), but not in the *BRAF*-wt samples (figure 6B, right panel).

To evaluate the clinical significance of these cell types, we evaluated relevant clinical factors (age, gender and AJCC stages) in a multivariate analysis model (figure 7). In the *BRAF*-mutant samples, increased CAFs were significantly associated with poor survival, whereas increased iTregs were significantly associated with improved survival (figure 7A). B cells were associated with a trend to improved survival (p=0.078) in the *BRAF*-mutant samples (figure 7A). In the *BRAF*-wt samples, advanced age and higher AJCC stage were significantly associated with poor survival (figure 7B). The predictive values of CAFs remained significant, whereas iTreg remained the same trend as in the *BRAF*-mutant samples but not significant (p=0.052) (figure 7B). Interestingly, Th2 immune cells were significantly associated with improved survival, while B cells showed no association with survival in the *BRAF*-wt samples (figure 7B). Taken together, CAFs and iTregs had prognostic value in melanoma regardless of *BRAF* mutation status, while B cells and Th2 immune cell populations were associated with improved survival in *BRAF*-mutant and *BRAF*-wt, respectively.

DISCUSSION

Melanoma is an aggressive form of skin cancer. Although it accounts for only 5% of all skin cancer cases, it leads to 80% of skin cancer-related deaths.[1] The development and progression of melanoma are based on the accumulation of genomic changes, including high ultraviolet-driven mutation burdens, which contribute to the development of melanoma and make it one of the most immunogenic tumors.[45] Hence, immunotherapy, such as ICIs, that harness and enhance the body's antitumor immune response have proven to be effective treatment strategies in patients with melanoma as adjuvant therapy after complete surgical resection[46] and in patients with

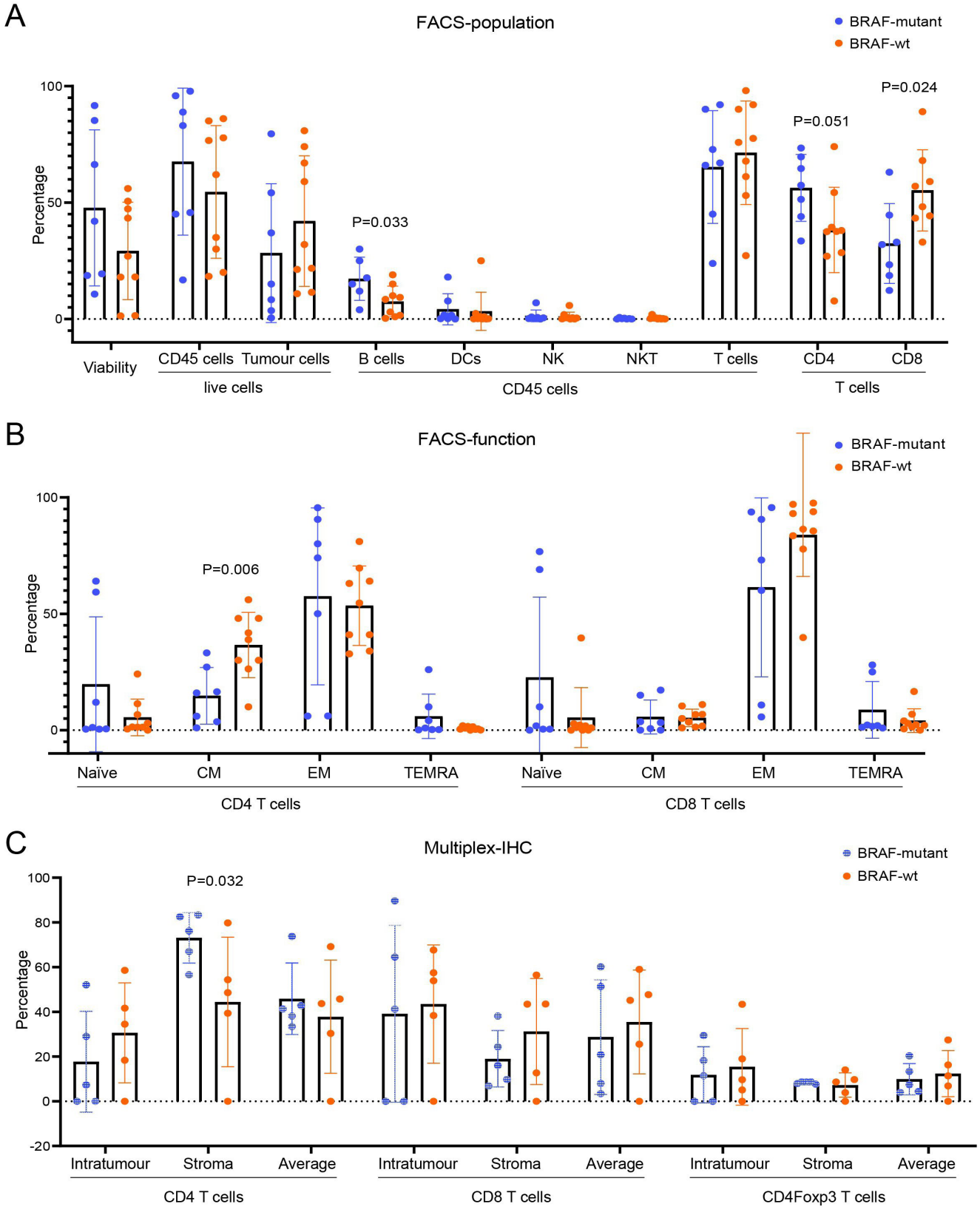

Figure 5 Evaluation of immune composition using flow cytometry and IHC methods. (A) Flow cytometry analysis of B cells, DCs, NK, NKT cells, T cells, $CD4^+$ T cells and $CD8^+$ T cells from seven *BRAF*-mutant samples and nine *BRAF*-wt samples. (B) Cell differentiation status (naive, CM, central memory; EM, effector memory; TEMRA, T effector memory with CD45RA) of $CD4^+$ T cells and $CD8^+$ T cells were analyzed by flow cytometry. (C) Multiplex IHC analysis to further characterize the distribution (IT, intratumor; stroma) of $CD4^+$ T cells, $CD8^+$ T cells and $CD4^+Foxp3^+$ T cells using five *BRAF*-mutant samples and five *BRAF*-wt samples. Each dot represents one melanoma sample, and data show mean±SEM. Statistical analyses were performed using a Mann-Whitney U test. P values are indicated. FACS, flow cytometry; IHC, immunohistochemistry; NK, natural killer.

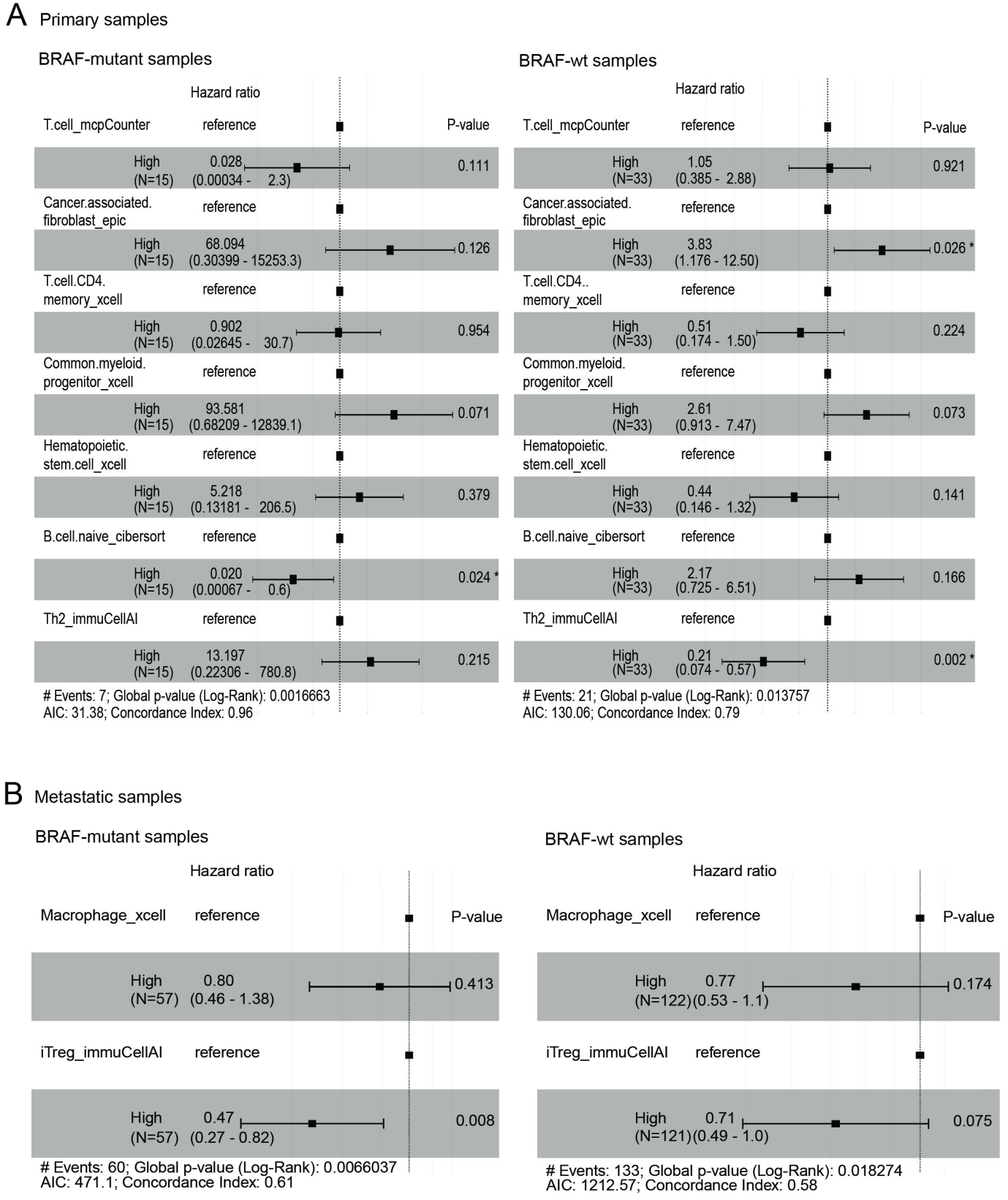

Figure 6 Survival analysis. Penalized Cox proportional hazard model was applied to the scores of cell type signature selected by the fwelnet model using the primary (A) and metastatic (B) TCGA SKCM cohorts. SKCM, skin cutaneous melanoma; TCGA, The Cancer Genome Atlas.

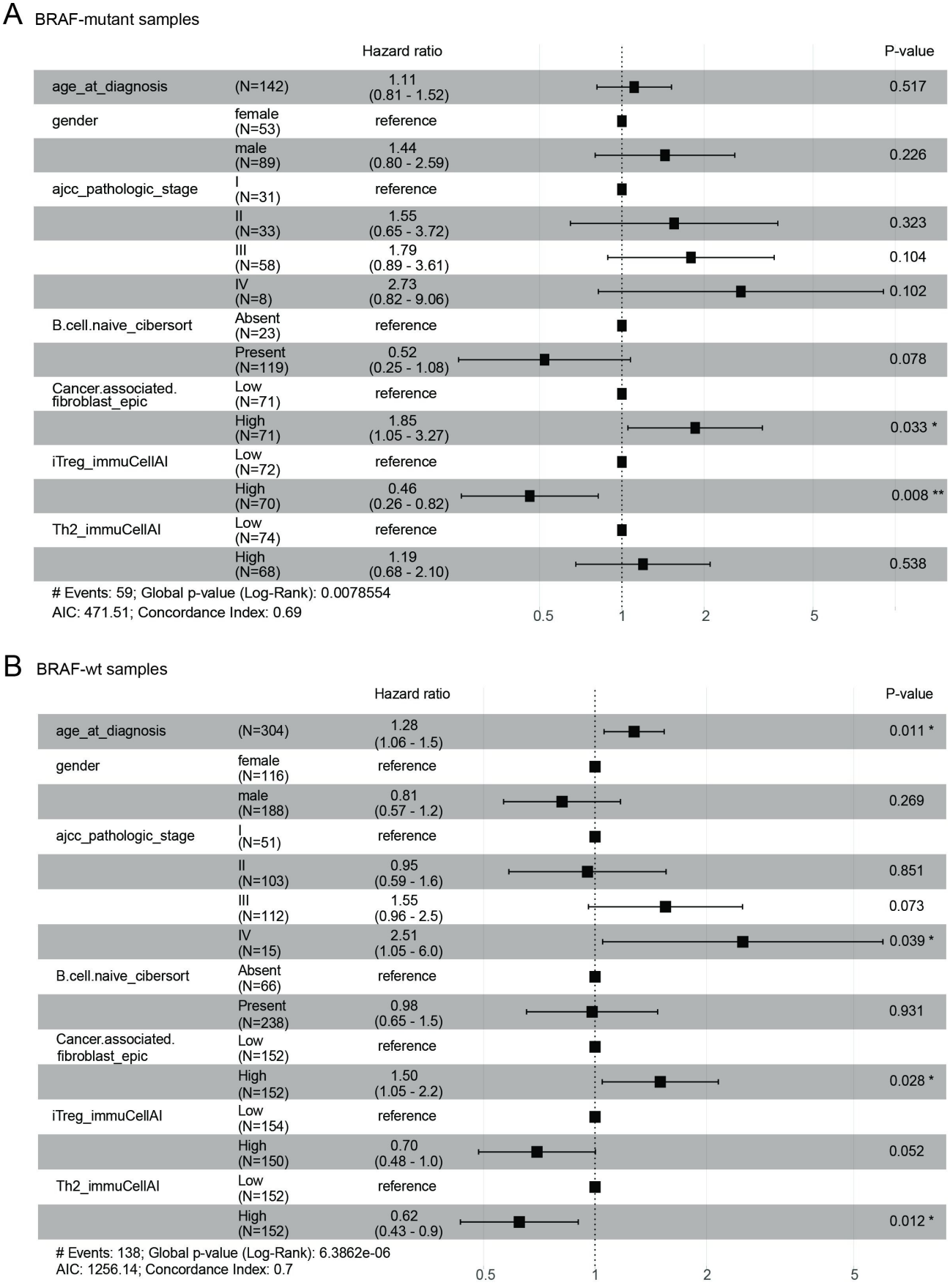

Figure 7 Multivariate survival analysis. The prognostic significances of cell types of interest were evaluated in *BRAF*-mutant melanoma (A) and *BRAF*-wt melanoma (B) when incorporating with other clinical factors (age, gender and AJCC stages). *P = <0.05, **P=<0.01.

advanced disease.[11 12] However, not all patients respond well to immunotherapy[11 12]; thus, understanding the immune microenvironment is necessary to optimize patient treatment plan. Indeed, patients with *BRAF*-mutant and *BRAF*-wt melanoma respond differentially to combination ICI therapy.[12]

In this study, in order to capture the extensive heterogeneity that exists in the tumor microenvironment of V600 *BRAF*-mutant and *BRAF*-wt melanoma samples, we used data from a range of melanoma cohorts. In addition, the datasets were generated by multiple approaches, including scRNA-seq, bulk RNA-seq, flow cytometry and multiplex IHC. We identified increased $CD4^+$ T cells (not significant in scRNA-seq) and B cells, but decreased $CD8^+$ T cells infiltrate in the *BRAF*-mutant metastatic melanoma samples, using scRNA-seq, bulk RNA-seq and flow cytometry approaches. Other cell types were not able to be estimated and validated across multiple platforms due to the limitations of cell preparations or characterization differences of cell phenotypes using different technologies. For example, Dabrosin *et al*[47] investigated the relationship between innate immune cell infiltration and *BRAF* mutation in 385 primary melanoma and 96 paired metastases using IHC and found that *BRAF*-positive primary tumors and metastases exhibited increased $CD123^+$ plasmacytoid DC numbers compared with *BRAF*-negative tumors. We did not observe this difference in the single-cell RNA sequencing and bulk-RNA sequencing cohorts, which could relate to the characterization difference between the IHC and sequencing technologies.

Increased $CD4^+$ T cells and B cell infiltration play a significant role in forming a protective antitumor response. Apart from producing cytokines and tumor-specific antibodies, intratumoral B cells are able to present B cell receptor-cognate antigens to $CD4^+$ T cells[48] and affect the clonality,[49] phenotype[50] and activation[51] of $CD4^+$ T cells in the tumor. The underlying mechanism whereby *BRAF* mutations in the tumor lead to increased B cells and $CD4^+$ T cells infiltration remains unknown.

The decrease of $CD8^+$ T cells infiltrate in melanoma with *BRAF* mutation was also observed in a Korean melanoma cohort.[52] Although the potential mechanisms of this observation remain obscure, one of our hypothesis is that *BRAF* mutations may be associated with decreased MHC-I expression and decreased tumor antigen presentation on the tumor surface.[53] Further validation with mutational status and MHC expression may provide more detailed insight to understand the mechanism of *BRAF* mutations in forming the melanoma microenvironment. Interestingly, Federick *et al*[54] demonstrated that treatment with either BRAF inhibitor alone or BRAF +MEK inhibitor was associated with an increased expression of melanoma antigens and an increase in $CD8^+$ T cells infiltrate. The finding was supported by another study showing that an influx of $CD8^+$ T cells occurs after triple BRAF +MEK therapy.[55] More specifically, a recent study using sequential tumor biopsies obtained before and during BRAF or MEK inhibitor demonstrated that treatment with BRAF/MEK inhibition in patients with melanoma allows an increased expansion of pre-existing melanoma-specific T cells by induction of T-box expressed in T cells (T-bet) and transcription factor-7 (TCF-7) in T cells.[56] T-bet and TCF-7 are two transcription factors required for self-renewal and persistence of $CD8^+$ memory T cells.[57] These studies point to one approach to overcome the reduced $CD8^+$ T cells in the *BRAF*-mutant microenvironment.

In this study, we further investigated the association of immune composition with the survival of patients with melanoma. CAFs and iTregs were shown to be associated with opposite outcomes in both *BRAF*-mutant and *BRAF*-wt melanoma. Interestingly, increased naive B cells were associated with a trend to improved survival (p=0.078) in patients with melanoma with *BRAF* mutations, but no association with survival was observed in the *BRAF*-wt samples. This finding was supported by another large-scale study (n=703), which investigated the individual B cell score in treatment-naive primary cutaneous melanomas.[58] The association between tumor-infiltrating B cells and improved patient survival has been demonstrated in other tumor types, such as lung adenocarcinoma,[59] hepatocellular carcinoma[60] and ovarian cancer.[61] The mechanistic role of B cells in antitumor surveillance and immunity remains largely unknown. One explanation could be the involvement of tertiary lymphoid structures (TLSs). TLSs are germinal centre-like follicle aggregates present in the tumor, with a B cell zone containing follicular dendritic cells and a T cell zone with mature dendritic cells.[62] These TLSs are thought to orchestrate both local and systemic antitumor responses and are able to generate both effector and memory T cells and B cells.[63] Naive B cells enter the TLSs follicle to initiate a germinal center reaction and differentiate into effector B cells, that is, memory B cells and plasma cells.[64] Recent data demonstrated that B cells and TLSs promote immunotherapy response.[65] The heterogeneous B cell subpopulations, including naive, follicular, memory plasmablasts and plasma B cells,[66] and the variety of antibodies secreted (IgG1, IgG2, IgG3, IgG4 and IgA) may exert differential influences in the tumor microenvironment and need to be comprehensively investigated.

In summary, we identified increased $CD4^+$ T cells and B cells but decreased $CD8^+$ T cells in *BRAF*-mutant melanoma samples, especially in the metastatic setting. Further work is required to characterize the phenotypes, antigen specificities and biological functions of these immune populations, as well as the underlying mechanisms leading to differential enrichment in *BRAF*-mutant versus wild-type melanomas. Recently, Aoude *et al*[67] reported an interesting association between CT—biomarker, mean of positive pixels and the tumor microenvironment in patients with melanoma. Non-invasive techniques, such as CT image parameters, are necessary for the development of prognostic or predictive biomarkers in late-stage patients. Further work is of interest to investigate the association between radiomics, such as CT image parameter, *BRAF* mutation status and the immune populations

in the tumor microenvironment. We anticipate that such efforts will drive the rational design of improved therapeutic interventions and combinations—both immune and molecular targeted—for patients with melanoma.

In conclusion, using an orthogonal approach we showed that the immune context of *BRAF* mutant was distinct from that of *BRAF*-wt melanoma, especially in the metastatic melanoma setting. We observed significantly increased B cells and CD4 $^{+}$ T cells in *BRAF*-mutant versus wild-type disease. In contrast, metastatic *BRAF*-wt melanoma had significantly increased CD8 $^{+}$ T cells versus *BRAF*-mutant disease. Our results also showed an association of increased naive B cells and Th2 cells with improved overall survival in *BRAF*-mutant and *BRAF*-wt melanoma, respectively. This study characterizing cell type compositions provides an opportunity to better understand the tumor microenvironment of *BRAF*-mutant and *BRAF*-wt melanoma samples and to tailor management for patients with melanoma.

Author affiliations
[1]Cancer Immunology Program, Peter MacCallum Cancer Centre, Melbourne, Victoria, Australia
[2]Sir Peter MacCallum Department of Oncology, University of Melbourne, Melbourne, Victoria, Australia
[3]Walter and Eliza Hall Institute of Medical Research, Melbourne, Victoria, Australia
[4]Department of Computing and Information Systems, University of Melbourne VCCC, Parkville, Victoria, Australia
[5]Centre for Cancer Immunotherapy, Peter MacCallum Cancer Centre, Melbourne, Victoria, Australia
[6]Division of Cancer Surgery, Peter MacCallum Cancer Centre, Melbourne, Victoria, Australia
[7]Department of Medical Oncology, Peter MacCallum Cancer Centre, Melbourne, Victoria, Australia
[8]The University of Sydney, Melanoma Institute Australia, Sydney, New South Wales, Australia
[9]Department of Tissue Pathology and Diagnostic Oncology, Royal Prince Alfred Hospital, Camperdown, New South Wales, Australia
[10]Melanoma Institute Australia, North Sydney, New South Wales, Australia
[11]Department of Medical Oncology, Royal North Shore Hospital, Sydney, New South Wales, Australia
[12]Faculty of Medicine and Health, The University of Sydney, Sydney, New South Wales, Australia
[13]Department of Medicine, Central Clinical School, Monash University, Clayton, Victoria, Australia

Twitter David E Gyorki @davidgyorki and Richard A Scolyer @Twitter @ProfRScolyerMIA

Acknowledgements The authors acknowledge the contribution of the Department of Health and Human Services acting through the Victorian Cancer Agency (The VCA project number TRP16020). The authors wish to thank Melanoma Research Victoria (MRV) and acknowledge the contributing MRV sites: Peter MacCallum Cancer Centre; Victorian Melanoma Service, Alfred Health; Olivia Newton-John Cancer Research Institute, Austin Health; Skin Health Institute; Border Medical Oncology Research Unit. Support from colleagues at Melanoma Institute Australia and Royal Prince Alfred Hospital are also gratefully acknowledged. Figure 1 was created with BioRender.com.

Contributors MJD and PJN designed the study. MW and SZ conducted experiments and performed the analysis. AP performed flow cytometry and analyzed the data. KT, DEG, GAM, RAS, GL, JSW, MCA, GA-Y, AW, SS and JAT curated the data. MW and SZ wrote the paper with input from all authors. All authors have read and agreed to the published version of the manuscript. PN acts as guarantor for the study.

Funding This study is funded by the Centre for Cancer Immunotherapy in Victoria Comprehensive Cancer Centre and receives support from the NHMRC program grant 1132373. RAS and GVL are supported by a National Health and Medical Research Council of Australia (NHMRC) Program Grant (APP1093017) and Practitioner Fellowships. GVL is supported by the University of Sydney Medical Foundation. MCA is supported by a National Health and Medical Research Council of Australia CJ Martin Early Career Fellowship (#1148680).

Competing interests RAS has received fees for professional services from Qbiotics, Novartis, Merck Sharp & Dohme, NeraCare, AMGEN, Bristol-Myers Squibb, Myriad Genetics, GlaxoSmithKline. GL has received professional consulting fees from Aduro Biotech, Amgen, Array Biopharma, Boehringer Ingelheim International GmbH, Bristol-Myers Squibb, Highlight Therapeutics SL, Merck Sharpe & Dohme, Novartis Pharma AG, Pierre Fabre, QBiotics Group, Regeneron Pharmaceuticals, SkylineDX BV (all unrelated to this work). PJN received research funding from Roche/Genentech, BMS, MSD, Allergan, Compugen, Crispr Therapeutics. The other authors declare no conflicts of interest.

Patient consent for publication Not applicable.

Ethics approval This study involves human participants and was approved by Peter MacCallum Cancer Center HREC approval number 07/38. Participants gave informed consent to participate in the study before taking part.

Provenance and peer review Not commissioned; externally peer reviewed.

Data availability statement Data are available upon reasonable request.

ORCID iDs
Minyu Wang http://orcid.org/0000-0002-1051-5855
Richard A Scolyer http://orcid.org/0000-0002-8991-0013
Miles C Andrews http://orcid.org/0000-0003-1231-8641
Paul Joseph Neeson http://orcid.org/0000-0002-2729-5887

REFERENCES

1 Schadendorf D, Hodi FS, Robert C, *et al*. Pooled analysis of long-term survival data from phase II and phase III trials of ipilimumab in unresectable or metastatic melanoma. *J Clin Oncol* 2015;33:1889–94.
2 Cancer Genome Atlas Network. Genomic classification of cutaneous melanoma. *Cell* 2015;161:1681–96.
3 Davies H, Bignell GR, Cox C, *et al*. Mutations of the BRAF gene in human cancer. *Nature* 2002;417:949–54.
4 Hodis E, Watson IR, Kryukov GV, *et al*. A landscape of driver mutations in melanoma. *Cell* 2012;150:251–63.
5 Curtin JA, Fridlyand J, Kageshita T, *et al*. Distinct sets of genetic alterations in melanoma. *N Engl J Med* 2005;353:2135–47.
6 Chapman PB, Hauschild A, Robert C, *et al*. Improved survival with vemurafenib in melanoma with BRAF V600E mutation. *N Engl J Med* 2011;364:2507–16.
7 Hauschild A, Grob J-J, Demidov LV, *et al*. Dabrafenib in BRAF-mutated metastatic melanoma: a multicentre, open-label, phase 3 randomised controlled trial. *Lancet* 2012;380:358–65.
8 Robert C, Grob JJ, Stroyakovskiy D, *et al*. Five-year outcomes with dabrafenib plus trametinib in metastatic melanoma. *N Engl J Med* 2019;381:626–36.
9 Larkin J, Ascierto PA, Dréno B, *et al*. Combined vemurafenib and cobimetinib in BRAF-mutated melanoma. *N Engl J Med* 2014;371:1867–76.
10 Dummer R, Ascierto PA, Gogas HJ, *et al*. Overall survival in patients with BRAF-mutant melanoma receiving encorafenib plus binimetinib versus vemurafenib or encorafenib (COLUMBUS): a

multicentre, open-label, randomised, phase 3 trial. *Lancet Oncol* 2018;19:1315–27.
11 Hamid O, Robert C, Daud A, *et al*. Five-year survival outcomes for patients with advanced melanoma treated with pembrolizumab in KEYNOTE-001. *Ann Oncol* 2019;30:582–8.
12 Larkin J, Chiarion-Sileni V, Gonzalez R, *et al*. Five-year survival with combined nivolumab and ipilimumab in advanced melanoma. *N Engl J Med* 2019;381:1535–46.
13 Dummer R, Brase JC, Garrett J, *et al*. Adjuvant dabrafenib plus trametinib versus placebo in patients with resected, $BRAF^{V600}$-mutant, stage III melanoma (COMBI-AD): exploratory biomarker analyses from a randomised, phase 3 trial. *Lancet Oncol* 2020;21:358–72.
14 Sumimoto H, Imabayashi F, Iwata T, *et al*. The BRAF-MAPK signaling pathway is essential for cancer-immune evasion in human melanoma cells. *J Exp Med* 2006;203:1651–6.
15 Khalili JS, Liu S, Rodríguez-Cruz TG, *et al*. Oncogenic BRAF(V600E) promotes stromal cell-mediated immunosuppression via induction of interleukin-1 in melanoma. *Clin Cancer Res* 2012;18:5329–40.
16 Hu-Lieskovan S, Mok S, Homet Moreno B, *et al*. Improved antitumor activity of immunotherapy with BRAF and MEK inhibitors in BRAF(V600E) melanoma. *Sci Transl Med* 2015;7:279ra41.
17 Proietti I, Skroza N, Michelini S, *et al*. BRAF inhibitors: molecular targeting and immunomodulatory actions. *Cancers* 2020;12:12071823. doi:10.3390/cancers12071823
18 Pires da Silva I, Wang KYX, Wilmott JS, *et al*. Distinct molecular profiles and immunotherapy treatment outcomes of V600E and V600K BRAF-mutant melanoma. *Clin Cancer Res* 2019;25:1272–9.
19 Tirosh I, Izar B, Prakadan SM, *et al*. Dissecting the multicellular ecosystem of metastatic melanoma by single-cell RNA-seq. *Science* 2016;352:189–96.
20 Lotfollahi M, Naghipourfar M, Luecken MD. Query to reference single-cell integration with transfer learning. *bioRxiv* 2020.
21 Wolf FA, Angerer P, Theis FJ. SCANPY: large-scale single-cell gene expression data analysis. *Genome Biol* 2018;19:15.
22 Colaprico A, Silva TC, Olsen C, *et al*. TCGAbiolinks: an R/Bioconductor package for integrative analysis of TCGA data. *Nucleic Acids Res* 2016;44:e71.
23 Robinson MD, Oshlack A. A scaling normalization method for differential expression analysis of RNA-seq data. *Genome Biol* 2010;11:R25.
24 Robinson MD, McCarthy DJ, Smyth GK. edgeR: a Bioconductor package for differential expression analysis of digital gene expression data. *Bioinformatics* 2010;26:139–40.
25 Chen Y, Lun ATL, Smyth GK. From reads to genes to pathways: differential expression analysis of RNA-Seq experiments using Rsubread and the edgeR quasi-likelihood pipeline. *F1000Res* 2016;5:1438.
26 Ritchie ME, Phipson B, Wu D, *et al*. limma powers differential expression analyses for RNA-sequencing and microarray studies. *Nucleic Acids Res* 2015;43:e47.
27 Thorsson V, Gibbs DL, Brown SD, *et al*. The immune landscape of cancer. *Immunity* 2019;51:411–2.
28 Finotello F, Mayer C, Plattner C, *et al*. Molecular and pharmacological modulators of the tumor immune contexture revealed by deconvolution of RNA-seq data. *Genome Med* 2019;11:34.
29 Li B, Severson E, Pignon J-C, *et al*. Comprehensive analyses of tumor immunity: implications for cancer immunotherapy. *Genome Biol* 2016;17:174.
30 Newman AM, Liu CL, Green MR, *et al*. Robust enumeration of cell subsets from tissue expression profiles. *Nat Methods* 2015;12:453–7.
31 Becht E, Giraldo NA, Lacroix L, *et al*. Estimating the population abundance of tissue-infiltrating immune and stromal cell populations using gene expression. *Genome Biol* 2016;17:218.
32 Aran D, Hu Z, Butte AJ. xCell: digitally portraying the tissue cellular heterogeneity landscape. *Genome Biol* 2017;18:220.
33 Racle J, de Jonge K, Baumgaertner P, *et al*. Simultaneous enumeration of cancer and immune cell types from bulk tumor gene expression data. *Elife* 2017;6. doi:10.7554/eLife.26476. [Epub ahead of print: 13 11 2017].
34 Miao Y-R, Zhang Q, Lei Q, *et al*. ImmuCellAI: a unique method for comprehensive T-cell subsets abundance prediction and its application in cancer immunotherapy. *Adv Sci* 2020;7:1902880.
35 Sturm G, Finotello F, Petitprez F, *et al*. Comprehensive evaluation of transcriptome-based cell-type quantification methods for immuno-oncology. *Bioinformatics* 2019;35:i436–45.
36 Friedman J, Hastie T, Tibshirani R. Regularization paths for generalized linear models via coordinate descent. *J Stat Softw* 2010;33:1–22.
37 Simon N, Friedman J, Hastie T, *et al*. Regularization paths for COX's proportional hazards model via coordinate descent. *J Stat Softw* 2011;39:1–13.
38 Tibshirani R, Bien J, Friedman J, *et al*. Strong rules for discarding predictors in lasso-type problems. *J R Stat Soc Series B Stat Methodol* 2012;74:245–66.
39 Tay K, Aghaeepour N, Hastie T. Feature-weighted elastic net: using" features of features" for better prediction. *arXivorg* 2020.
40 Tay JK, Aghaeepour N, Hastie T. Feature-weighted elastic net: using "features of features" for better prediction. *arXivorg*2020.
41 Halse H, Colebatch AJ, Petrone P, *et al*. Multiplex immunohistochemistry accurately defines the immune context of metastatic melanoma. *Sci Rep* 2018;8:11158.
42 Therneau TM, Grambsch PM. *Modeling survival data: extending the COX model*. New York, NY: Springer, 2000.
43 survminer: Drawing Survival Curves using'ggplot2'. [program]. 0.4.8 version 2017.
44 Subramanian A, Tamayo P, Mootha VK, *et al*. Gene set enrichment analysis: a knowledge-based approach for interpreting genome-wide expression profiles. *Proc Natl Acad Sci U S A* 2005;102:15545–50.
45 Blankenstein T, Coulie PG, Gilboa E, *et al*. The determinants of tumour immunogenicity. *Nat Rev Cancer* 2012;12:307–13.
46 Eggermont AMM, Blank CU, Mandala M, *et al*. Adjuvant pembrolizumab versus placebo in resected stage III melanoma. *N Engl J Med* 2018;378:1789–801.
47 Dabrosin N, Sloth Juul K, Bæhr Georgsen J, *et al*. Innate immune cell infiltration in melanoma metastases affects survival and is associated with BRAFV600E mutation status. *Melanoma Res* 2019;29:30–7.
48 Rivera A, Chen CC, Ron N, *et al*. Role of B cells as antigen-presenting cells in vivo revisited: antigen-specific B cells are essential for T cell expansion in lymph nodes and for systemic T cell responses to low antigen concentrations. *Int Immunol* 2001;13:1583–93.
49 Zhu W, Germain C, Liu Z, *et al*. A high density of tertiary lymphoid structure B cells in lung tumors is associated with increased $CD4^+$ T cell receptor repertoire clonality. *Oncoimmunology* 2015;4:e1051922.
50 Bruno TC, Ebner PJ, Moore BL, *et al*. Antigen-presenting intratumoral B cells affect $CD4^+$ TIL phenotypes in non-small cell lung cancer patients. *Cancer Immunol Res* 2017;5:898–907.
51 Bouaziz J-D, Yanaba K, Venturi GM, *et al*. Therapeutic B cell depletion impairs adaptive and autoreactive CD4+ T cell activation in mice. *Proc Natl Acad Sci U S A* 2007;104:20878–83.
52 Min K-W, Choe J-Y, Kwon MJ, *et al*. BRAF and NRAS mutations and antitumor immunity in Korean malignant melanomas and their prognostic relevance: gene set enrichment analysis and CIBERSORT analysis. *Pathol Res Pract* 2019;215:152671.
53 Bradley SD, Chen Z, Melendez B, *et al*. BRAFV600E co-opts a conserved MHC class I internalization pathway to diminish antigen presentation and CD8+ T-cell recognition of melanoma. *Cancer Immunol Res* 2015;3:602–9.
54 Frederick DT, Piris A, Cogdill AP, *et al*. BRAF inhibition is associated with enhanced melanoma antigen expression and a more favorable tumor microenvironment in patients with metastatic melanoma. *Clin Cancer Res* 2013;19:1225–31.
55 Ascierto PA, Ferrucci PF, Fisher R, *et al*. Dabrafenib, trametinib and pembrolizumab or placebo in BRAF-mutant melanoma. *Nat Med* 2019;25:941–6.
56 Peiffer L, Farahpour F, Sriram A, *et al*. BRAF and MEK inhibition in melanoma patients enables reprogramming of tumor infiltrating lymphocytes. *Cancer Immunol Immunother* 2021;70:1635–47.
57 Jansen CS, Prokhnevska N, Master VA, *et al*. An intra-tumoral niche maintains and differentiates stem-like CD8 T cells. *Nature* 2019;576:465–70.
58 Nsengimana J, Laye J, Filia A, *et al*. β-Catenin-mediated immune evasion pathway frequently operates in primary cutaneous melanomas. *J Clin Invest* 2018;128:2048–63.
59 Isaeva OI, Sharonov GV, Serebrovskaya EO, *et al*. Intratumoral immunoglobulin isotypes predict survival in lung adenocarcinoma subtypes. *J Immunother Cancer* 2019;7:279.
60 Shi J-Y, Gao Q, Wang Z-C, *et al*. Margin-infiltrating CD20(+) B cells display an atypical memory phenotype and correlate with favorable prognosis in hepatocellular carcinoma. *Clin Cancer Res* 2013;19:5994–6005.
61 Nielsen JS, Sahota RA, Milne K, *et al*. CD20+ tumor-infiltrating lymphocytes have an atypical CD27- memory phenotype and together with CD8+ T cells promote favorable prognosis in ovarian cancer. *Clin Cancer Res* 2012;18:3281–92.
62 Dieu-Nosjean M-C, Goc J, Giraldo NA, *et al*. Tertiary lymphoid structures in cancer and beyond. *Trends Immunol* 2014;35:571–80.

63 Sautès-Fridman C, Lawand M, Giraldo NA, *et al*. Tertiary lymphoid structures in cancers: prognostic value, regulation, and manipulation for therapeutic intervention. *Front Immunol* 2016;7:407.
64 Germain C, Gnjatic S, Dieu-Nosjean M-C. Tertiary lymphoid structure-associated B cells are key players in anti-tumor immunity. *Front Immunol* 2015;6:67.
65 Helmink BA, Reddy SM, Gao J, *et al*. B cells and tertiary lymphoid structures promote immunotherapy response. *Nature* 2020;577:549–55.
66 Maecker HT, McCoy JP, Nussenblatt R. Standardizing immunophenotyping for the human immunology project. *Nat Rev Immunol* 2012;12:191–200.
67 Aoude LG, Wong BZY, Bonazzi VF, *et al*. Radiomics biomarkers correlate with CD8 expression and predict immune signatures in melanoma patients. *Mol Cancer Res* 2021;19:950–6.